Energetic, electronic and optical properties of lanthanide doped TiO_2: An *ab initio* LDA+*U* study

Winfred M. Mulwa[1,*], Cecil N.M.Ouma[2], Martin O. Onani[3], Francis B. Dejene[1]

[1]*Department of physics, University of the Free State-Qwaqwa Campus, Private Bag X13, Phuthaditjhaba, 9866, South Africa*

[2]*Natural Resources and Environment, Council for Scientific and Industrial Research, P.O. Box 395, Pretoria,0001, South Africa*

[3]*Chemistry Department, University of the Western Cape, Private Bag X17, Bellville, Cape Town, South Africa*

Abstract

Substitutional energies, thermodynamic charge transition levels and optical properties of lanthanide doped anatase TiO_2 has been investigated using local density approximation with the Hubbard *U* correction (LDA+*U*) within the density functional theory formalism. All the lanthanides apart from La introduced impurity states in the host band gap on doping. The calculated substitutional energies indicate that it is possible to dope TiO_2 with lanthanide ions. The optimal doping percentage was predicted to be ~3% and dopant levels resulting from Ce, Nd, Sm, Gd and Tm doping were found to possess negative U characteristics. In addition the calculated thermodynamic transition levels predicted Lu as not having any possible charge transitions within the host band gap. The calculated optical absorption coefficients indicate that lanthanide doping led to optical absorption in the visible regime.

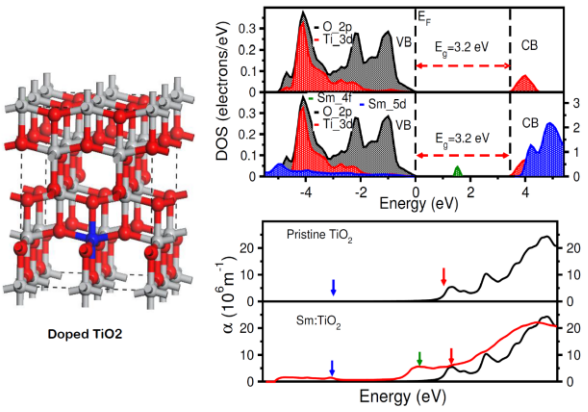

***Keywords*:** Doped-TiO_2, anatase, rutile, dopant levels, DFT+*U*, optical properties

*Corresponding author: Tel +27(0) 84-359-4493, e-mail: COuma@csir.co.za, moronaphtaly84@gmail.com

1.0 Introduction

Titanium dioxide (TiO_2) has vast applications in electronics, energy and photonics among other applications [1]. One of the key applications is photocatalysis where solar energy is converted into hydrogen energy via the splitting of water, decomposing toxic organic and inorganic pollutants to purify water and air, and providing super-hydrophilicity to solid surfaces [2]. TiO_2, a wide band gap compound semiconductor, is known to be active only in the ultraviolet (UV) region of the photoemission spectrum. However, in order for TiO_2 to fully utilize the major part of the solar spectrum, besides UV which is just 5% of the solar spectrum, several studies aimed at improving the properties of TiO_2 via doping and co-doping TiO_2 with various elements have been carried out with varied measures of success [3]. TiO_2 has rutile, anatase and brookite polymorphs. Rutile and brookite are direct band gap semiconductors. The higher photocatalytic activity of the anatase TiO_2 over the rutile and brookite polymorphs can be attributed to the indirect band gap of the anatase which leads to a slow decay lifetime of photoexcited charge carriers.[1]

Good photocatalysts are known to have conduction band edges that are more negative than the reduction (redox) potential of water. However, visible-light photocatalysts have been found to be either unstable under light illumination (CdSe) [4] or have low activity (Fe_2O_3) [5]. Attempts have been made in trying to use transition metal (TM) oxides such as Cr_2O_3 as photocatalysts since they have good visible light absorption [6]. Experimentally, Cr_2O_3 has a band gap of 3.4 eV [7] which is larger than the experimental band gap of rutile. This explains why Cr_2O_3 conduction band edges were found to be more negative compared to the redox potential of water [8]. Therefore, incorporating a dopant into TiO_2, in such a way that the conduction band levels are made more negative than the redox potential of water can facilitate the visible light absorption of the host oxide under visible irradiation.

The most widely used semiconductor photo-catalyst is titanium dioxide (TiO_2), because it is relatively easy and inexpensive to synthesize, it is highly stable under irradiation conditions, non-toxic, and can completely degrade several classes of pollutants in aqueous and gas phases [2,3]. However, its success as a semiconductor photo-catalyst is limited by its wide band-gap (3.2 eV) and the recombination of the photogenerated electron-hole pairs [4]. A 3.2 eV (387 nm) band gap necessitates the use of UV light in the photo-production of electrons and holes.

Conflicting reports exist in the literature regarding the photocatalytic activities on semiconductors doped with transition metal ions [5]. The disparities are due to a number of reasons including; variability in the synthetic procedures employed for the preparation of catalysts which lead to the formation of photo catalysts with varying physio-chemical characteristics, varying experimental conditions used in the photocatalytic reactions and the different quantitative methods used for analysis of reactant or product concentrations[6]. In recent times, Herrmann *et al*.,[7] made a compelling argument that both *n*- and *p*-doping by transition metal ions leads to an increase in the recombination rate of the photogenerated electron-hole pairs. In recent years, anion doping has gained popularity and the prime motivation in this direction has been in extending the visible light response of large band-gap semiconductors[8,9].

It has been reported that TiO_2 co-doped with La^{3+} and Eu^{3+} exhibits better photocatalytic properties compared to that of pristine TiO_2[10]. The improved photocatalytic properties

resulted from transitions of 4*f* electrons in the dopants. A similar observation was made when TiO_2 was doped with lanthanides[11,12]. Doping TiO_2 with lanthanides has been the subject of intense investigation both experimentally [11–14] and theoretically[15–17]. This is because lanthanide doping could remarkably improve the photocatalytic activity of TiO_2 as it registers visible light response as well as strong redox potential at the same time. Lanthanides are among the rare-earth elements with great luminescent properties. They are characterized by the 4*f* orbitals which in some cases are shielded by filled $5p^6 6s^2$ sub orbitals leading to very important spectroscopic properties[18] however, lanthanides ions are not excited efficiently without a host [19]. Their properties are known to greatly depend on their electronic configuration and ionic radius, which decreases steadily along the lanthanide series with respect to the fillings of the 4*f* orbitals[20].

Density functional theory (DFT) has been the basis for most of the electronic structure calculations, however it has limitations when it comes to describing properties such as band gaps (see ref [21–24]). Another key shortcoming of standard DFT is that it cannot accurately describe systems with strong correlation effects. This is because within DFT, the electron–electron interaction is expressed as the sum of the Hartree and exchange-correlation (XC) terms however, the XC term is usually approximated. Due to this approximation, the XC term cannot accurately account for electronic interactions in strongly correlated systems, hence the need for DFT+*U* technique where a Hubbard correction *U* is added to the standard DFT formalism [25,26].

In this study we investigate lanthanide doped anatase TiO_2 using density functional theory with Hubbard *U* correction (DFT+*U*) because lanthanides are known to have 4*f* orbitals which cannot be accurately described using standard DFT. The electronic and optical properties of anatase doped TiO_2 with each of the eleven (11) different lanthanides namely: La, Ce, Pr, Nd, Pm, Sm, Eu, Gd, Tm, Yb and Lu has been investigated. In addition we have also calculated the dopant substitutional energies, thermodynamic charge transitions energies as well as their optical absorption spectra.

2.0 Calculation models and methods

Projector augmented plane wave (PAW) method [27] as implemented in the Quantum ESPRESSO code[28], has been used to study the properties of interest within the DFT+*U* formalism. PAW potentials were used for Ti, O and all the lanthanides investigated in this study. PAW is an improvement to the pseudopotential approximation as it combines the pseudopotential approximation with linearized augmented-plane-wave (LAPW) method[29,30], making PAW more accurate compared to the pseudopotential approximation. The Brillouin zone of the unit cell of anatase TiO_2 was sampled using a converged Monkhorst-Pack [31] k-point mesh of 6x6x3 and kinetic energy cut-off of 80 Ry. Standard DFT is known to severely underestimate the band gap in semiconductors, in the case of TiO2, the band gap of anatase TiO_2 obtained using spin polarized local density approximation (LDA) was found to be 1.89 eV compared to the experimental value of 3.2 eV [32]. This underestimation stems from the wrong energy position of the 3*d* orbitals of Ti within the pseudopotential description which intern courses (spurious) interaction with the O *sp* bands. To correct for the band gap underestimation in standard LDA, we have adopted the methodology of [33–35] where an *ad hoc* Hubbard *U* potential is included in the DFT+*U* scheme. Within this formalism, the Hubbard *U* values used should not be considered as empirical parameters introduced to correct the gap and not the physical on-site electron-

electron screened potentials, in the sense of the many-body Hubbard Hamiltonian. The unphysical Ti_{3d}-O_{2sp} is overcome by including a Hubbard potential *U* = 10 eV on 3*d* orbital of Ti and 5 eV on the 2*p* orbital of O was found to produce the experimental of gap of TiO2. A similar approach was used to obtain *U* values for the lanthanide ions whereby we used lanthanide sesquioxides varied the Hubbard term until a band gap close to experimental value is arrived at. The experimental data used was obtained from [36–38]. The obtained values of *U* for the case of lanthanides were found to be consistent with other studies [36].

The calculated equilibrium parameters were; a = 3.792Å c/a = 2.502, which were in good agreement with experimental values, a = 3.785Å and c/a = 2.513[39], as well as another theoretical LDA+*U* results, a = 3.819Å and c/a = 2.502 [40]. After obtaining the equilibrium structure, 72 atom supercells were constructed from the equilibrium structure. The choice of the 72 atom supercell was made by calculating the dopant substitutional energy as function of supercell size up to 288 atoms, the substitutional energy difference between the 72 atom unit cell and the 288 atom unit cell was found to be ~1 eV thus due to computational efficiency, the 72 atom unit was preferred. Doping was then done by substituting Ti atoms with lanthanide atoms. In order to avoid significant dopant-dopant interaction within the lattice, lanthanide atoms were introduced at the next-nearest Ti atom sites from the site of the first substitution until the desired dopant concentration was achieved. The atomic positions of the supercells containing the dopants were then relaxed keeping the volume constant. Figure 1 shows a supercell containing a dopant within its lattice.

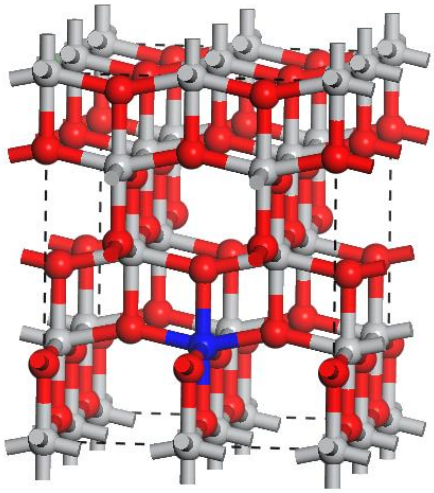

Figure 1: (Colour online) A supercell of doped anatase TiO2 (Red, Grey and Blue balls represents O, Ti and dopant atoms respectively).

2.1 Optical properties

The response function for the optical properties of a solid, describing the absorption or emission of electrons or photons is the dielectric function. From the imaginary part of the dielectric function, it is possible to obtain some of the optical properties of a solid. In this study, the optical properties have been obtained through the frequency-dependent dielectric function, $\varepsilon(\omega)=\varepsilon_1(\omega)+i\varepsilon_2(\omega)$ using the formalism of Ehrenreich and Cohen[41]. Within this formalism, the imaginary part of the dielectric function is given as:

$$\varepsilon_2(\omega)=\frac{4\pi^2e^2\hbar}{m^2\omega^2}\sum_{vc}\frac{2}{(2\pi)^2}\int_{BZ}\delta[\omega_{cv}(k)-\omega]|M_{cv}(k)|^2d^3k \qquad 1.0$$

where the integral is over the first Brillouin zone, $M_{cv}(k)=\langle u_{ck}|\hat{e}.\nabla|u_{ck}\rangle$ are the dipole matrix elements for the direct transitions between valence and conduction bands states. $\hbar\omega_{cv}(k)=E_{ck}-E_{vk}$ is the excited energy, $\hat{e}$ is the polarization vector of the electric field, and $u_{ck}(r)$ is the periodic part of the Bloch wave function for a conduction band state with wave vector *k*. Although DFT is known to underestimate the band gap of semiconductors, our results show that optical properties obtained using DFT outputs are surprisingly in good agreement with experiment. This is attributed to the ability of the local density approximation to yield accurate matrix elements between occupied and empty states.

In this study our first goal was to determine the doping percentage that would yield visible light absorption in TiO_2 since high concentrations may lead to low photocatalytic activity. Large impurity states in the band gap that act as recombination centres for photoexcited electron-hole pairs. To achieve this, some of the optically active lanthanide elements namely; Gd, Eu and Sm were used to determine this optimal doping percentage. This was done by plotting the optical absorption of spectrum of TiO_2 doped with each of the chosen lanthanide ions individually at different concentrations as seen in Figure 2. From the figure, it can be seen that the doping percentage that led to absorption on the visible regime is 2.7778% (~3.0%) which is within the experimental doping percentage range [35].

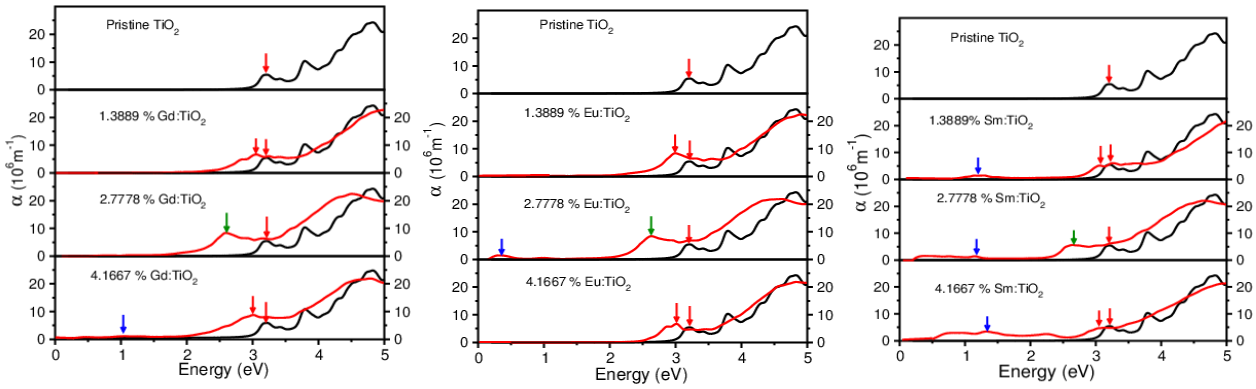

Figure 2: (Colour online) Calculated absorption spectra of TiO_2 doped with different lanthanide elements at different percentage concentrations. (Red, Green and Blue arrows represent UV, visible and IR absorption peaks respectively).

Table 1: Extracted absorption coefficient of doped anatase TiO_2.

Ln:TiO_2	dopant	*U* (eV)	Absorption peaks (ev)		Absorption peaks (nm)		
0%			3.2		387.5		UV
1.3889%	Gd	2	3.1		400		UV
	Eu	3	3.1		400		UV
	Sm	2	1.1 3.1	1127	400	IR	UV
2.7778%	Gd	2	2.6		476		Visible
	Eu	3	0.4 2.6	3100	476	IR	Visible
	Sm	2	1.1 2.6	1127	476	IR	Visible
4.1667%	Gd	2	1.1 3.1	1127	400	IR	UV
	Eu	3	3.1		400		UV
	Sm	2	1.3 3.1	953	400	IR	UV

After obtaining the doping percentage that lead to absorption in the visible regime, substitutional energies, electronic properties and optical properties for all the dopants were obtained at this dopant percentage (~3.0%).

2.2 Dopant Substitutional energies

According to the Zhang–Northrup[42] formalism, the dopant substitutional energy at any given charge state q can be obtained as

$$E^{q}_{\text{dopant}} = E_{\text{undoped}} - E_{\text{doped}} + n\mu_{\text{Ti}} - n\mu_{\text{dopant}} + q\left(E_{\text{VBM}} + E_{\text{Fermi}}\right) + E^{q}_{\text{corr}} \qquad 2.0$$

where E_{undoped} is the total energy of pristine TiO_2, E_{doped} is the total energy of the lanthanide doped TiO_2, μ_{Ti} and μ_{dopant} are the chemical potentials of Ti and dopant respectively, n is the number of atoms substituted or added to the supercell, E_{VBM} and E_{Fermi} are the energy of the valence band maximum and fermi energy respectively and E^{q}_{corr} is the correction made to calculated substitutional energies due to finite size errors and image charge corrections obtained using the charge model of Freysoldt *et al*.[43,44]. $E_{corr} = E_{\text{iso}} - E_{\text{per}} - q\Delta V_{q/b}$, E_{iso} is the self-energy of the isolated charge distribution, E_{per} the electrostatic energy of the system subject to periodic boundary conditions and $q\Delta V_{q/b}$ is the potential alignment term. The calculated substitutional energies at different charge sates are presented in Table 2.

2.2 Thermodynamic transition levels

Using the calculated substitutional energies, it is possible to obtain the thermodynamic charge transition level $\varepsilon^{q/q'}$ which is defined as the Fermi energy position where a dopant in two different charge states has the same dopant substitutional (formation) energy[45]. This can be obtained for say 0 and +1 charge states as follows.

$$\varepsilon^{0/+1} = \frac{\left(E^{+1}_{\text{dopant}} - E^{0}_{\text{dopant}}\right)}{\left((0) - (+1)\right)} \qquad 3.0$$

where E^{+1}_{dopant} and E^{0}_{dopant} are the dopant substitutional energies for +1 and 0 charge states obtained using equation 2. Additionally the same thermodynamic charge transition levels can be obtained by making plots of dopant substitutional energies as functions of the Fermi level position as presented in Figure 3. In the figure, the gradient of each line is the defect charge state, and the intersection of two lines is the thermodynamic charge transition level of the defect. The thermodynamic charge transition levels can be associated to defect levels observed from deep level transient spectroscopy (DLTS) or temperature dependent Hall measurements[45].

3.0 Results and Discussions

3.1 Substitutional energies

Dopant substitutional energies were calculated using equation (2.0). In order to bench mark our calculation with previous studies[46,47]. We have calculated the dopant substitutional energies at ~1.4% doping (one (1) atom lanthanide substitution) in the neutral charge state so as to compare our methodology to previous studies (see Table 1). From the table it can be seen that our results are consistent previous studies when it comes to the order of which atom easily dopes anatse TiO2 i.e. Ce < Gd < Pr < Eu. There is difference in the substitutional energies compared to previous studies, this can be attributed to [47] not using the Hubbard term in the study and [46] using different values of U on the lanthanides compared to the ones used in this study. The different values of U resulted from using different experimental results used to bench mark/ callibrate the Hubbard term.

Table 1 *Substitutional energies and averaged bond lengths of ~1.4% Ln-doped TiO_2.*

			Substitutional energy (eV)		Bond lengths	
At. No.	Atom	*U* (eV)	This work	Other works	Ti-O (Å)	Ln-O (Å)
58	Ce	3	-1.73	-2.2[46], 1.58[47]	1.912	1.981
59	Pr	2	0.62	1.4[46], 2.83[47]	1.916	1.991
63	Eu	3	3.08	10.5[46], 5.52[47]	1.911	1.971
64	Gd	2	-1.44	0.2[46], 1.76[47]	1.922	1.982
	TiO_2				1.901	

We then proceeded using equation 2.0, to calculate the dopant substitutional energies at ~3.0 dopant concentration percentage (two (2) atom lanthanide substitution) (see Table 2. From the table it can be seen that the substitutional energies varies depending on the charge state. It can also be seen from the table that it is easy to dope TiO_2 with a mojority lanthanide elements since the dopant substitutional energies are relatively low (=< 3 eV) hence the reason why lanthanide doped TiO_2 have attracted lots of experimental scrutiny. Ce and Gd had the lowest substitutional energies compared to the rest of the lanthanides. Their formation energies were also negative indication the ease of doping anatase TiO_2 with Ce and Gd. This consistent with [46,47] as well as an experimental study that reported Ce as having the highest photo-catalytic activity in TiO_2 [48]. The order of the dopant substitutional energies in ascending order are as follows; Ce < Gd < Pr < Pm < Nd < Lu < La < Yb < Tm < Eu. This order is also consistent with ab initio results of [47].

We then calculated the dopant substitutional energies a function of the Fermi level also using equation 2.0 and the results are presented in Figure 3. As earlier mentioned, the intersection of any two lines in each of the figures, that is, the Fermi level position at which the dopant substitutional energies of the dopant in two different charge states are equal. This was also confirmed using equation 3.0. From Figure 3 it is evident that thermodynamic transitions resulting from the doped systems occur very close to the valence band maximum (VBM), about 1.5 eV above the VBM, Equation 3.0 was then used to identify the possible transitions associated with the doped systems (see Table 3) than may be observed experimentally through DLTS measurements.

Table 2 *Substitutional energies of ~3.0% Ln-doped TiO_2 at different charge states under Ti-rich conditions.*

Atm. No	Dopant	*U* (eV)	-3	-2	-1	0	1	2	3
57	La	2	3.35	3.05	2.75	2.48	2.14	1.80	1.53
58	Ce	3	0.15	-0.17	-0.95	-1.31	-1.63	-2.22	-2.69
59	Pr	2	1.59	1.36	1.11	0.86	0.59	0.32	0.02
60	Nd	3	2.26	2.06	1.86	1.66	1.46	1.26	1.06
61	Pm	1.5	1.96	1.73	1.48	1.21	0.94	0.67	0.54
62	Sm	2	3.53	3.30	3.05	2.91	2.64	2.39	2.12
63	Eu	3	4.00	3.76	3.51	3.26	3.01	2.67	2.54
64	Gd	2	-0.40	-0.63	-0.88	-1.13	-1.30	-1.54	-1.74
69	Tm	2	5.82	5.28	4.78	2.84	2.39	2.35	2.31
70	Yb	2	3.32	3.09	2.94	2.81	2.54	2.31	2.04
71	Lu	3.5	2.52	2.29	1.99	1.72	1.59	1.25	0.98

Table 3 *Calculated thermodynamic charge transition levels in eV of ~3.0% Ln-doped TiO_2 refferenced to the valence band maximum (VBM).*

At. No.		(+3/+2)	(+1/0)	(0/-1)	(-2/-3)	(0/-2)	(-1/-3)
57	La	--	--	--	0.30	0.28	--
58	Ce	0.47	--	--	--	--	--
59	Pr	--	--	--	--	--	--
60	Nd	--	--	0.20	--	--	0.20
61	Pm	--	--	--	--	0.26	0.24
62	Sm	--	--	--	--	--	--
63	Eu	0.13	0.25	--	0.23	0.25	--
64	Gd	--	--	--	--	--	--
69	Tm	--	--	0.45	--	--	--
70	Yb	--	--	--	--	--	--
71	Lu	--	--	--	0.23	0.29	--

As can be seen from the Table, Pr, Sm, Gd, Yb had no possible thermodynamic charge transition levels. A survey of present available literature indicate that no DLTS measurements have been done of the lanthanide doped TiO2 however, the absence of thermodynamic charge transition levels can in part be attributed to the inadequacies of standard DFT/DFT+U when it comes to defect studies[49] hence the need for techniques beyond the one used in this present study. Ce, Nd, Sm, Gd and Tm had levels that exhibited negative U characteristic. A defect has negative-U properties if it can trap two electrons (or holes) with the second being bound more strongly than the first [50]. How these negative U defects affect the photocatalytic properties of doped TiO_2 is still an open question.

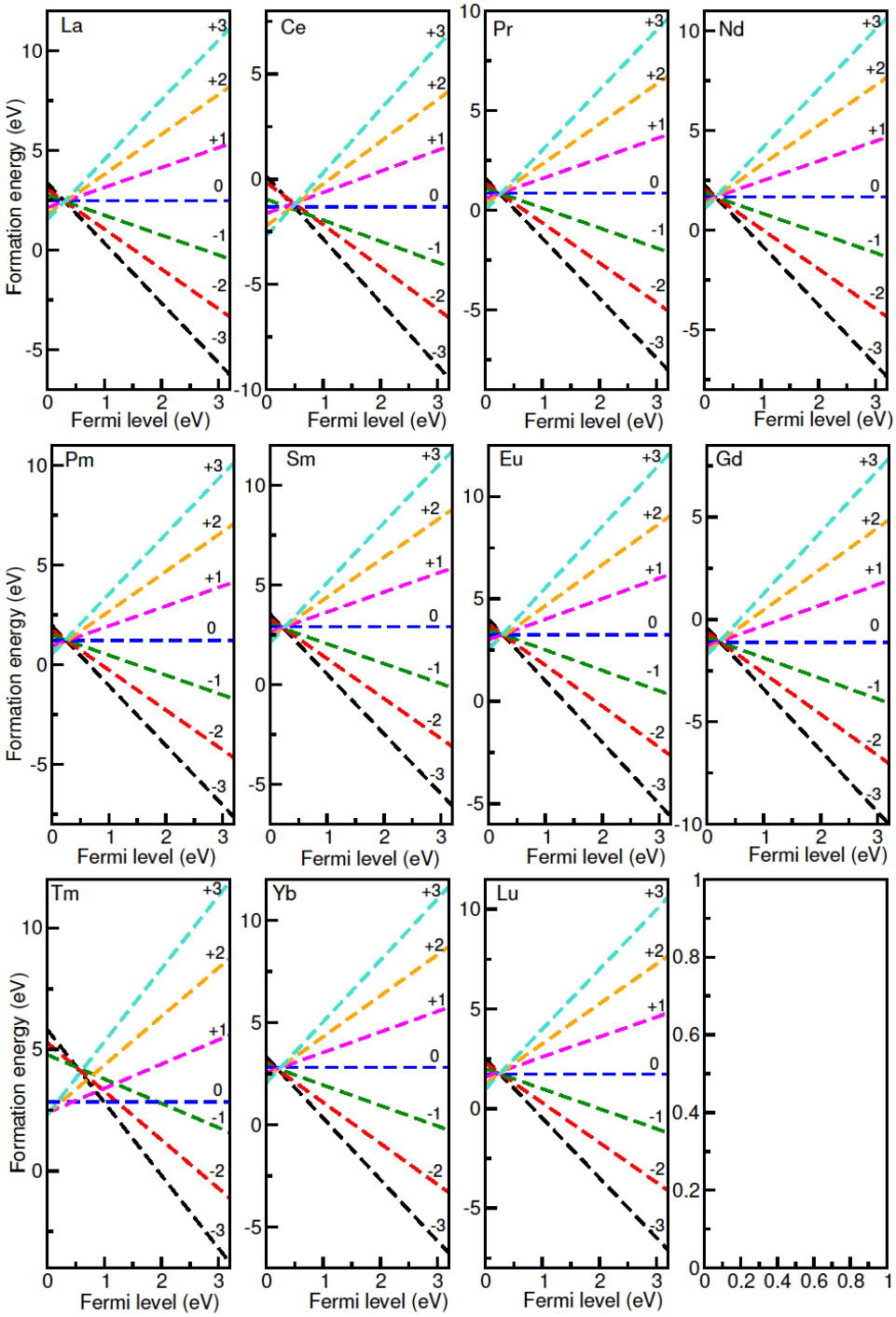

Figure 3: *(Colour online) Calculated substitutional energies of doped TiO_2 as a function of the Fermi level.*

3.2 Electronic properties

In order to understand the electronic properties of doped TiO_2, we calculated and obtained the projected density of states using LDA+*U*. As can be seen in Figure 4, the band gap of pristine TiO_2 is 3.2 eV and it is characterized by Ti 3*d* and O 2*p* orbitals in valence and conduction band respectively. On doping TiO_2, there is hybridization of Ti 3*d* and O 2*p* with the dopant states, there was no hybridization between the O 2*p* states or Ti 3*d* states with 4*f*

states when TiO_2 is doped with La (see Figure 4 a)). Figure 4 also shows four sets of results as a consequence of the location of the impurity levels within the host band gap.

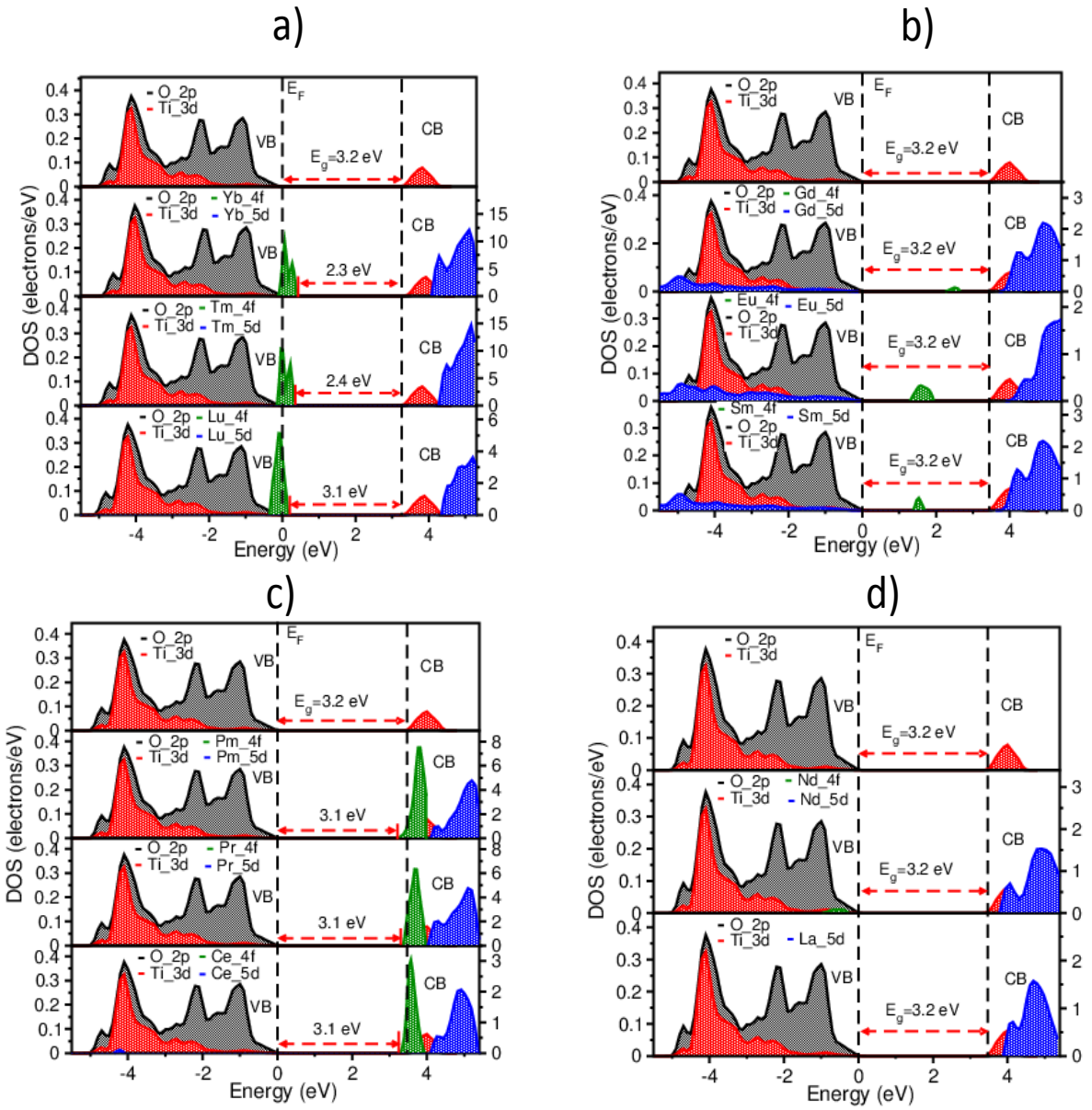

Figure 4: *(Colour online) Calculated projected density of states of doped TiO_2.*

It can be seen from Figure 4 that, as the atomic number increases from La to Lu, the energy level of the impurity states shifts from conduction band (La,Ce,Pr,Nd,Pm) through the middle of the band gap (Sm,Eu,Gd) to the valence band (Tm,Yb,Lu). It can also be seen in the case of Sm, Eu and Gd (see Figure 3 b)) that the dopant impurity levels are inside the band gap of TiO_2. It therefore implies in these three cases that, if photon energy is absorbed, the electrons in the valence band will first be excited to the new states (impurity states) and finally excited to the conduction band. From the PDOS of La, Pr and Nd it can be seen in Figure 3 a) and b) that they don't introduce any impurity states within the band gap TiO_2. Although Pr and Nd have dopant the states deep in the conduction band, La was found not to be having the 4*f* states an observation also made by [51]. Lu, Yb and Tm introduced acceptor states while Ce and Pm introduced donor states within the band gap of TiO_2 as

seen in Figures 3 a), 3 b) and 3 c) which are likely the source of absorption peaks that lead to visible light absorption in doped TiO_2.

Similar to previous studies [47], it was observed in this study that doping anatse TiO_2 with lanthanide ions resulted in delocalized 4*f* states and that it is these delocalized 4*f* states that produce impurity energy levels within the band gap. The 4*f* states were found not to hybridize with either the O 2*p* states or Ti 3*d* states unlike the case of transition metal doped TiO_2 [17]. The impurity energy levels due to the delocalized 4*f* states are broader than peaks of transition metal-doped TiO_2 this is consistent with what was observed by [47] and the reason for this broadening was explained as resulting from 4*f* states possessing seven orbits for electrons to occupy. Another consistency with [47] was observed in the comparison doped and undoped anatase TiO_2 where PDOS of doped TiO_2 were broader in comparison to the undoped. This was attributed to the reduction of crystal symmetry which results in electronic nonlocality [52].

3.3 Optical properties

The optical properties of a semiconductor are mainly determined by its electronic structure, because of this, we investigated the relationship between electronic structure and optical properties of lanthanide-doped TiO_2 systems.

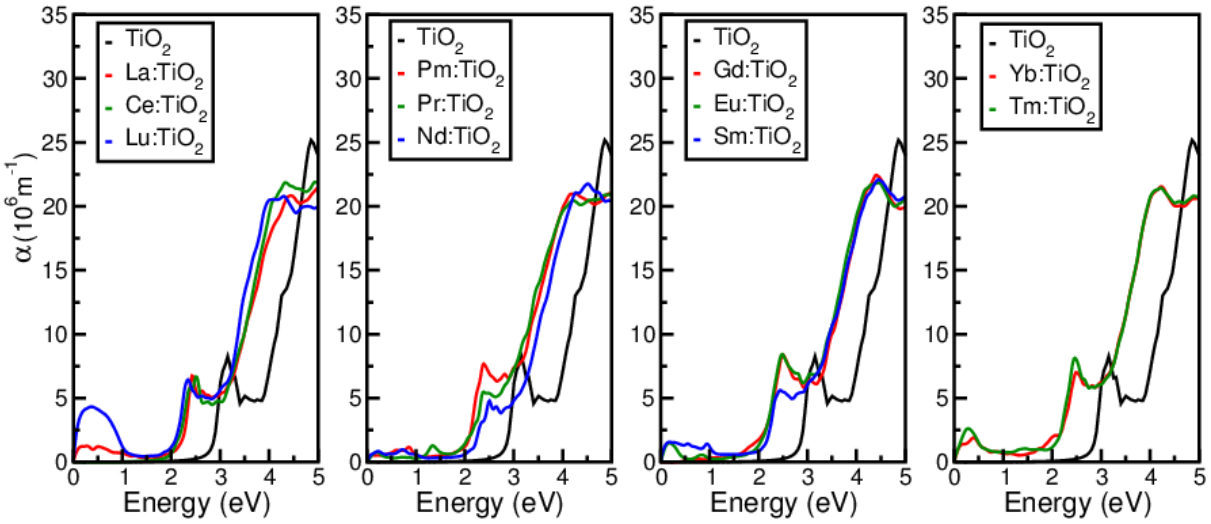

Figure 5: *Optical absorption spectra of Ln:TiO_2*

***Table 4**: Extracted absorption coefficients of Ln:TiO_2.*

Ln:TiO_2	U (eV)	Absorption peaks (eV)		Absorption peaks (nm)			
0%			3.2		387.5	UV	
La	2	0.6	2.5	2066.7	496	IR	Visible
Ce	3		2.5		496		Visible
Pr	2	1.4	2.4	885.7	516.7	IR	Visible
Nd	3	0.7	2.4	1771.4	516.7	IR	Visible
Pm	1.5	0.8	2.4	1550	516.7	IR	Visible
Sm	2	1.0	2.6	1240	476.9	IR	Visible
Eu	3	1.0	2.6	1240	476.9	IR	Visible
Gd	2		2.6		476.9		Visible
Tm	2	0.4	2.5	3100	496	IR	Visible
Yb	2	0.4	2.5	3100	496	IR	Visible
Lu	3.5	0.4	2.4	3100	516.7	IR	Visible

As seen in Figure 4 from the PDOS of Pristine TiO_2, the band gap of anatase TiO_2 was found to be 3.2 eV, which is consistent with the optical absorption coefficient presented in Figure 5 and Table 4. Pristine TiO_2 had an optical absorption peak at 3.2 eV (388 nm) which is in the UV region in conformity with experimental results [53]. This peak at 388 nm was used as benchmark to locate the other peaks resulting from lanthanide-doped TiO_2. For an orderly discussion on absorption coefficients, of lanthanide doped TiO_2, using the impurity state position we have come up four categories.

Category I: Impurity states located at or around the valence band maximum (VBM) (Yb, Tm and Lu). The 4*f* impurity states of the lanthanides are at the top of the VB and new absorption peaks were observed to occur at 2.5 eV (496 nm) for Yb and Tm and 2.4 eV (516.7 nm) for Lu owing to the narrowing of the band gap as shown in Figure 5. This was consistent with experimental results [54,55] where absorption peaks were of Yb, Tm and Lu were observed at 2.6 eV (476 nm), 2.75 eV (450 nm) and 2.8 eV (442 nm) respectively where all dopant led to peaks in the visible regime. The difference in energies might be attributes the exchange-correlation functional which is an approximated term within the DFT formalism.

Category II: Impurity states withinin the band gap region of the host (Gd, Eu and Sm). When the lanthanides are in the octahedral discrete point charges field, the crystal field theory necessitates the intraband transition of lanthanide 4*f* electronic states [56]. Due to the position of the impurity states around the mid gap region of the host band gap, and the intraband transitions, the absorption coefficient peaks of Sm, Eu and Gd were found to shift absorption peak of the host from 3.2 eV (388 nm) which is in UV region to the visible light region at 2.6 eV (476.9 nm) as also shown in Figure 5 in agreement with [57–59] where the absorption peaks of Gd, Eu and Sm were observed at 2.0 eV (620 nm).

Category III: Impurity states at/around conduction band minimum (CBM) (Pm, Pr and Ce). The impurity states of Pm Pr and Ce were found to adequately cover the CBM resulting in the narrowing the bandgap to 3.1 eV which facilitates the shifting of absorption peaks from 3.2 eV (388 nm) in the pristine TiO_2 to 2.4 eV (516.7 nm) after both Pm and Pr doping and to 2.5 eV (496 nm) on Ce doping as seen in Figure 5. These results are in good agreement with experimental results [60,61] in which the absoption peaks on Pm, Pr and Ce absorption were observed at 2.8 eV (442 nm) for Pm and Pr while for Ce the peak was at 2.9 eV (422 nm).

Category IV: Clean band gap (Nd and La) the 4*f* states of Nd are found right inside the VB resulting in reduction in electronic occupation O 2*p*. The crystal field effect thus facilitates the shifting of absorption coefficient of the unsdoped host into the visible region at around 2.4 eV (516.7 nm). This was also in agreement with experimental results [62] where the absorption peak resulting from Nd doping was observed at 2.57 eV (482 nm). In the case of La doping, no impurity states from the 4*f* states were observed either within the band gap or at/around VBM or CBM however on ploting the absorption spectrum of the La-doped system, an optical absorption peak in the visible region at 2.5 eV (496 nm) was observed. There is no explanation in literature on why La behaves in this manner it has only be report that it has an "exceptional phenomena [51]".

Conclusions

We have investigated the electronic and optical properties of pristine anatase TiO_2 as well as lanthanides doped TiO_2 in addition substitutional energies of one atom and two atom substitution were investigated using DFT calculations applying LDA+*U* method. Ce and Gd had the least substitution energy in all charge states. The calculated thermodynamic transition levels exhibited negative U behaviour in the case of Ce, Nd, Sm, Gd and Tm. An optimal doping concentration was realized at 2.78% (~3.00%) which was within the experimental doping range. Doping TiO_2 with lanthanide ions was fund to results in shifying the absorption peaks of the of the pristine for the UV into the the visible regime. Lanthanide doping in TiO_2 was also found to lead to narrowing of the band gap(i.e. red shift). From our study there was consistency between calculated electronic and optical properties of both the pristine and lanthanide doped TiO_2 to both the observed experiemental results as well as other theoretical investigations.

Acknowledgement

This work is based on the research supported in part by the National Research Foundation of South Africa. The Grant holder acknowledges that opinions, findings and conclusions or recommendations expressed in any publication generated by the NRF supported research are that of the author(s) and that the NRF accepts no liability whatsoever in this regard.

References

[1] J. Zhang, P. Zhou, J. Liu, J. Yu, New understanding of the difference of photocatalytic activity among anatase, rutile and brookite TiO2, Phys. Chem. Chem. Phys. 16 (2014) 20382–20386.

[2] I.K. Konstantinou, T.A. Albanis, Photocatalytic transformation of pesticides in aqueous titanium dioxide suspensions using artificial and solar light: intermediates and degradation pathways, Appl. Catal. B Environ. 42 (2003) 319–335.

[3] Y. Zhang, Z.-R. Tang, X. Fu, Y.-J. Xu, TiO2- graphene nanocomposites for gas-phase photocatalytic degradation of volatile aromatic pollutant: is TiO2- graphene truly different from other TiO2- carbon composite materials?, ACS Nano. 4 (2010) 7303–7314.

[4] M. Ni, M.K.H. Leung, D.Y.C. Leung, K. Sumathy, A review and recent developments in photocatalytic water-splitting using TiO2 for hydrogen production, Renew. Sustain. Energy Rev. 11 (2007) 401–425.

[5] M.D. Hernández-Alonso, F. Fresno, S. Suárez, J.M. Coronado, Development of alternative photocatalysts to TiO 2: challenges and opportunities, Energy Environ. Sci. 2 (2009) 1231–1257.

[6] M. Yan, F. Chen, J. Zhang, M. Anpo, Preparation of controllable crystalline titania and study on the photocatalytic properties, J. Phys. Chem. B. 109 (2005) 8673–8678.

[7] J.-M. Herrmann, Fundamentals and misconceptions in photocatalysis, J. Photochem. Photobiol. A Chem. 216 (2010) 85–93.

[8] Z. Zhang, X. Wang, J. Long, Q. Gu, Z. Ding, X. Fu, Nitrogen-doped titanium dioxide visible light photocatalyst: spectroscopic identification of photoactive centers, J. Catal. 276 (2010) 201–214.

[9] R. Long, N.J. English, Tailoring the electronic structure of TiO 2 by cation codoping from hybrid density functional theory calculations, Phys. Rev. B. 83 (2011) 155209.

[10] A.B. Yusov, V.P. Shilov, Photochemistry of f-element ions, Russ. Chem. Bull. 49 (2000) 1925–1953.

[11] D.M. Tobaldi, A.S. Škapin, R.C. Pullar, M.P. Seabra, J.A. Labrincha, Titanium dioxide modified with transition metals and rare earth elements: Phase composition, optical properties, and photocatalytic activity, Ceram. Int. 39 (2013) 2619–2629.

[12] S.H.I. Huixian, T. Zhang, W. Hongliang, Preparation and photocatalytic activity of La 3+ and Eu 3+ co-doped TiO 2 nanoparticles: photo-assisted degradation of methylene blue, J. Rare Earths. 29 (2011) 746–752.

[13] K.T. Ranjit, I. Willner, S.H. Bossmann, A.M. Braun, Lanthanide oxide doped titanium dioxide photocatalysts: effective photocatalysts for the enhanced degradation of salicylic acid and t-cinnamic acid, J. Catal. 204 (2001) 305–313.

[14] K.T. Ranjit, I. Willner, S.H. Bossmann, A.M. Braun, Lanthanide oxide-doped titanium dioxide photocatalysts: novel photocatalysts for the enhanced degradation of p-chlorophenoxyacetic acid, Environ. Sci. Technol. 35 (2001) 1544–1549.

[15] S. Matsuo, N. Sakaguchi, K. Yamada, T. Matsuo, H. Wakita, Role in photocatalysis and coordination structure of metal ions adsorbed on titanium dioxide particles: a comparison between lanthanide and iron ions, Appl. Surf. Sci. 228 (2004) 233–244.

[16] D. Li, N. Ohashi, S. Hishita, T. Kolodiazhnyi, H. Haneda, Origin of visible-light-driven photocatalysis: a comparative study on N/F-doped and N--F-codoped TiO 2 powders

by means of experimental characterizations and theoretical calculations, J. Solid State Chem. 178 (2005) 3293–3302.

[17] T. Umebayashi, T. Yamaki, H. Itoh, K. Asai, Analysis of electronic structures of 3d transition metal-doped TiO 2 based on band calculations, J. Phys. Chem. Solids. 63 (2002) 1909–1920.

[18] J.-C.G. Bünzli, C. Piguet, Taking advantage of luminescent lanthanide ions, Chem. Soc. Rev. 34 (2005) 1048–1077.

[19] B.M. Tissue, Synthesis and luminescence of lanthanide ions in nanoscale insulating hosts, Chem. Mater. 10 (1998) 2837–2845.

[20] W. Liu, W. Küchle, M. Dolg, Ab initio pseudopotential and density-functional all-electron study of ionization and excitation energies of actinide atoms, Phys. Rev. A. 58 (1998) 1103.

[21] J. Paier, M. Marsman, K. Hummer, G. Kresse, I.C. Gerber, J.G. Angyán, Screened hybrid density functionals applied to solids., J. Chem. Phys. 124 (2006) 154709. doi:10.1063/1.2187006.

[22] J. Heyd, G.E. Scuseria, M. Ernzerhof, Hybrid functionals based on a screened Coulomb potential, J. Chem. Phys. 118 (2003) 8207. doi:10.1063/1.1564060.

[23] X. Ren, Beyond LDA and GGA - Tackling exact exchange , hybrid functional , MP2 , and RPA with numeric atom-centered orbitals The Fritz-Haber-Institute ab initio molecular simulations package, (2009).

[24] C.N.M. Ouma, M.Z. Mapelu, N.W. Makau, G.O. Amolo, R. Maezono, Quantum Monte Carlo study of pressure-induced B3-B1 phase transition in GaAs, Phys. Rev. B. 86 (2012) 104115. doi:10.1103/PhysRevB.86.104115.

[25] B. Himmetoglu, A. Floris, S. de Gironcoli, M. Cococcioni, Hubbard-corrected DFT energy functionals: The LDA+U description of correlated systems, Int. J. Quantum Chem. 114 (2014) 14–49. doi:10.1002/qua.24521.

[26] M. Cococcioni, S. De Gironcoli, Linear response approach to the calculation of the effective interaction parameters in the LDA+ U method, Phys. Rev. B. 71 (2005) 35105.

[27] G. Kresse, D. Joubert, From ultrasoft pseudopotentials to the projector augmented-wave method, Phys. Rev. B. 59 (1999) 1758–1775. doi:10.1103/PhysRevB.59.1758.

[28] P. Giannozzi, S. Baroni, N. Bonini, M. Calandra, R. Car, C. Cavazzoni, et al., QUANTUM ESPRESSO: A Modular and Open-Source Software Project for Quantum Simulations of Materials, J. Phys. Condens. Matter. 21 (n.d.) 395502.

[29] O.K. Andersen, Linear methods in band theory, Phys. Rev. B. 12 (1975) 3060–3083. doi:10.1103/PhysRevB.12.3060.

[30] D.D. Koelling, G.O. Arbman, Use of energy derivative of the radial solution in an augmented plane wave method: application to copper, J. Phys. F Met. Phys. 5 (1975) 2041–2054. doi:10.1088/0305-4608/5/11/016.

[31] H.J. Monkhorst, J.D. Pack, No Title, 13 (1976) 5188–5192.

[32] H. Tang, H. Berger, P.E. Schmid, F. Levy, G. Burri, Photoluminescence in TiO 2 anatase single crystals, Solid State Commun. 87 (1993) 847–850.

[33] A. Janotti, D. Segev, C. Van de Walle, Effects of cation d states on the structural and electronic properties of III-nitride and II-oxide wide-band-gap semiconductors, Phys. Rev. B. 74 (2006) 045202. doi:10.1103/PhysRevB.74.045202.

[34] A. Calzolari, M.B. Nardelli, Dielectric properties and Raman spectra of ZnO from a first principles finite-differences/finite-fields approach, Sci. Rep. 3 (2013).

[35] A. Calzolari, A. Ruini, A. Catellani, Anchor Group versus Conjugation: Toward the Gap-State Engineering of Functionalized ZnO ($10\bar{1}0$) Surface for Optoelectronic Applications, J. Am. Chem. Soc. 133 (2011) 5893–5899.

[36] R. Gillen, S.J. Clark, J. Robertson, Nature of the electronic band gap in lanthanide oxides, Phys. Rev. B. 87 (2013) 125116.

[37] A. V Prokofiev, A.I. Shelykh, B.T. Melekh, Periodicity in the band gap variation of Ln 2 X 3 (X= O, S, Se) in the lanthanide series, J. Alloys Compd. 242 (1996) 41–44.

[38] S. Kimura, F. Arai, M. Ikezawa, Optical study on electronic structure of rare-earth sesquioxides, J. Phys. Soc. Japan. 69 (2000) 3451–3457.

[39] T. Arlt, M. Bermejo, M.A. Blanco, L. Gerward, J.Z. Jiang, J.S. Olsen, et al., High-pressure polymorphs of anatase TiO 2, Phys. Rev. B. 61 (2000) 14414.

[40] M.E. Arroyo-de Dompablo, A. Morales-García, M. Taravillo, DFT+ U calculations of crystal lattice, electronic structure, and phase stability under pressure of TiO2 polymorphs, J. Chem. Phys. 135 (2011) 54503.

[41] H. Ehrenreich, M.H. Cohen, Self-consistent field approach to the many-electron problem, Phys. Rev. 115 (1959) 786.

[42] S. Zhang, J. Northrup, Chemical potential dependence of defect formation energies in

GaAs: Application to Ga self-diffusion, Phys. Rev. Lett. 67 (1991) 2339–2342. doi:10.1103/PhysRevLett.67.2339.

[43] C. Freysoldt, J. Neugebauer, C.G. Van de Walle, Electrostatic interactions between charged defects in supercells, Phys. Status Solidi. 248 (2011) 1067–1076. doi:10.1002/pssb.201046289.

[44] C. Freysoldt, J. Neugebauer, C. Van de Walle, Fully Ab Initio Finite-Size Corrections for Charged-Defect Supercell Calculations, Phys. Rev. Lett. 102 (2009) 016402. doi:10.1103/PhysRevLett.102.016402.

[45] C.G. Van de Walle, First-principles calculations for defects and impurities: Applications to III-nitrides, J. Appl. Phys. 95 (2004) 3851. doi:10.1063/1.1682673.

[46] W. Chen, P. Yuan, S. Zhang, Q. Sun, E. Liang, Y. Jia, Electronic properties of anatase TiO 2 doped by lanthanides: A DFT+ U study, Phys. B Condens. Matter. 407 (2012) 1038–1043.

[47] Z. Zhao, Q. Liu, Effects of lanthanide doping on electronic structures and optical properties of anatase TiO2 from density functional theory calculations, J. Phys. D. Appl. Phys. 41 (2008) 85417.

[48] Y. Du, M. Du, Y. Qiao, J. Dai, J. Xu, P. Yang, Ce (4+) doped TiO2 thin films: Characterization and photocatalysis, Colloid J. 69 (2007) 695–699.

[49] A. Janotti, C.G. Van de Walle, LDA + U and hybrid functional calculations for defects in ZnO, SnO2, and TiO2, Phys. Status Solidi. 248 (2011) 799–804. doi:10.1002/pssb.201046384.

[50] G.D. Watkins, Negative-U properties for defects in solids, in: Adv. Solid State Phys., Springer, 1984: pp. 163–189.

[51] W. Guan, F. Ji, Z. Xie, R. Li, N. Mei, Preparation and Photocatalytic Performance of Nano-TiO 2 Codoped with Iron III and Lanthanum III, J. Nanomater. (2015).

[52] G. Shao, Electronic structures of manganese-doped rutile TiO2 from first principles, J. Phys. Chem. C. 112 (2008) 18677–18685.

[53] G.K. Boschloo, A. Goossens, J. Schoonman, Photoelectrochemical study of thin anatase TiO2 films prepared by metallorganic chemical vapor deposition, J. Electrochem. Soc. 144 (1997) 1311–1317.

[54] M. Pal, U. Pal, R. Silva Gonzalez, E. Sanchez Mora, P. Santiago, Synthesis and photocatalytic activity of Yb doped TiO2 nanoparticles under visible light, in: J. Nano Res., 2009: pp. 193–200.

[55] K. Binnemans, Lanthanide-based luminescent hybrid materials, Chem. Rev. 109 (2009) 4283–4374.

[56] B. Henderson, G.F. Imbusch, Optical Spectroscopy of Inorganic SolidsOxford University Press, Oxford, 1989.

[57] M.A. Farrukh, M. Shahid, I. Muneer, S. Javaid, M. Khaleeq-ur-Rahman, Influence of gadolinium precursor on the enhanced red shift of Gd/SnO2--TiO2 nanoparticles and catalytic activity, J. Mater. Sci. Mater. Electron. (n.d.) 1–9.

[58] A. Podhorodecki, G. Zatryb, P. Sitarek, J. Misiewicz, D. Kaczmarek, J. Domaradzki, et al., Excitation mechanism of europium ions embedded into TiO 2 nanocrystalline matrix, Thin Solid Films. 517 (2009) 6331–6333.

[59] Q. Xiao, Z. Si, Z. Yu, G. Qiu, Sol--gel auto-combustion synthesis of samarium-doped TiO 2 nanoparticles and their photocatalytic activity under visible light irradiation, Mater. Sci. Eng. B. 137 (2007) 189–194.

[60] J. Reszczynska, D.A. Esteban, M. Gazda, A. Zaleska, Pr-doped TiO2. The effect of metal content on photocatalytic activity, Physicochem. Probl. Miner. Process. 50 (2014) 515–524.

[61] A. Malik, S. Hameed, M.J. Siddiqui, M.M. Haque, M. Muneer, Influence of Ce Doping on the Electrical and Optical Properties of TiO 2 and Its Photocatalytic Activity for the Degradation of Remazol Brilliant Blue R, Int. J. Photoenergy. 2013 (2013).

[62] D. Nassoko, Y.-F. Li, J.-L. Li, X. Li, Y. Yu, Neodymium-Doped with Anatase and Brookite Two Phases: Mechanism for Photocatalytic Activity Enhancement under Visible Light and the Role of Electron, Int. J. Photoenergy. 2012 (2012).